NMR Chemical Shifts. 3. A Comparison of Acetylene, Allene, and the Higher Cumulenes

Kenneth B. Wiberg,* Jack D. Hammer, Kurt W. Zilm,* and James R. Cheeseman

Department of Chemistry, Yale University, New Haven, Connecticut 06520-8107

Received March 9, 1999

The ^{13}C NMR shieldings for acetylene, allene, and some higher cumulenes have been calculated at the MPW1PW91/6-311+G(2d,p) level using both the GIAO and IGAIM procedures. The calculations satisfactorily reproduce the tensor components of the shielding for both acetylene and allene, including the remarkably large difference in the components about the long axes of these molecules. A linear molecule such as acetylene has no paramagnetic shielding about the symmetry axis. The strong diamagnetic shielding about this axis for acetylene results in part from the energetically and spatially degenerate π-orbitals. With allene, the π-orbitals are energetically degenerate, but are not spatially degenerate, and as a result they cannot be mixed and cannot give a shielding diamagnetic term. Instead, in the presence of a magnetic field, they mix with virtual orbitals, leading to a downfield paramagnetic term. The shieldings for all the compounds are analyzed on an MO basis.

Introduction

Acetylene (**1**) and allene (**2**) present an interesting contrast in their ^{13}C NMR spectra. Despite having the same sp + 2p hybridization at the acetylenic and the central allenic carbons, about its long axis (*z*) acetylene is more shielded than TMS by 90 ppm, whereas allene is deshielded by 180 ppm.[1] Why is there such a large difference between these carbons? We shall make use of ab initio calculations of the chemical shifts to cast light on this question. Other comparisons will be concerned with allene, butatriene (**4**), and other cumulenes. The comparison among the cumulenes will indicate whether the shifts for **2** are characteristic of cumulenes as a group.

Geometry optimizations were carried out at the MP2/6-311+G* level which has been found to satisfactorily reproduce the structures of the types of compounds in this paper (Table 1).[2] The calculations of the NMR shielding were carried out using the MPW1PW91 density functional model[3] using the 6-311+G(2d,p) basis set (or 6-311G(2d,p) for pentatetraene and hexapentaene which would not converge when diffuse functions were included).[4] The MPW1PW91 hybrid density functional was chosen because we have found it to give a better agreement with experiment than the more commonly used B3LYP density functional.[5] Both GIAO[6] and IGAIM[7] were used in the shielding calculations and gave essentially the same results.[8] Only the IGAIM results will be given below.

Table 1. MP2(full)/6-311+G* Calculated Energies and Structures

compound	energy (H)	structure
acetylene	−77.13416	r(C≡C) = 1.219, r(C−H) = 1.067
allene	−116.33442	r(C=C) = 1.313, r(C−H) = 1.085
butatriene	−154.31863	r(C_1=C_2) = 1.325, r(C_2−C_3) = 1.273, r(CH) = 1.086
pentatetraene	−192.30650	r(C_1=C_2) = 1.322, r(C_2−C_3) = 1.283, r(CH) = 1.087
hexapentaene	−230.29526	r(C_1=C_2) = 1.327, r(C_2−C_3) = 1.276, r(C_3−C_4) = 1.295

Acetylene and Allene

The MPW1PW91/6-311+G(2d,p) calculations using the MP2/6-311+G* geometries reproduce the experimental shielding data[1] in a satisfactory fashion for **1** and **2** (Table 2). One would not expect exact agreement since the calculations are for the gas phase whereas the experimental data were obtained in the solid phase. It was found that the addition of f functions at carbon or d functions at hydrogens had no significant effect on the calculated nuclear shielding. With all of the compounds, the long axis will be denoted as *z*. The shielding along an axis was decomposed into the contributions from the occupied MOs as described previously,[9,10] and the diamagnetic and paramagnetic terms were obtained separately.

(1) Zilm, K. W.; Grant, D. M. *J. Am. Chem. Soc.* **1981**, *103*, 2913. Beeler, A. J.; Orendt, A. M.; Grant, D. M.; Cutts, P. W.; Michl, J.; Zilm, K. W.; Downing, J. W.; Facelli, J. C.; Schindler, M. S.; Kutzelnigg, W. *J. Am. Chem. Soc.* **1984**, *106*, 7672,.

(2) Allene C=C bond length is 1.309 Å (Butcher, R. J.; Jones, W. J. *J. Raman Spectrosc.* **1973**, *1*, 393); acetylene C≡C bond length is 1.203 Å (Berry, R. J.; Harmony, M. D. *Struct. Chem.* **1990**, *1*, 49).

(3) Adamo, C.; Barone, V. *J. Chem. Phys.* **1998**, *108*, **664**. Perdew, J. P.; Burke, K.; Wang, Y. *Phys. Rev.* **1996**, *B54*, 16533.

(4) In the other cases we examined, removal of the diffuse functions led to only a 1−2 ppm change in the shielding.

(5) Wiberg, K. B. *J. Comput. Chem.*, in press.

(6) Ditchfield, R. *Mol. Phys.* **1974**, *27*, 789. Wolinksi, K.; Hinton, J. F.; Pulay, P. *J. Am. Chem. Soc.* **1990**, *112*, 8251. Cheeseman, J. R.; Trucks, G. W.; Keith, T. A.; Frisch, M. J. *J. Chem. Phys.* **104**, *14*, 1996

(7) Keith, T. A.; Bader, R. F. W. *Chem. Phys. Lett.* **1992**, *194*, 1. Keith, T. A.; Bader, R. F. W. *Chem. Phys. Lett.* **1993**, *210*, 223. Unlike the GIAO method, IGAIM makes use of field-free molecular orbitals.

(8) Some representative isotropic shielding values are diacetylene, GIAO 114.1 and 119.9 ppm; IGAIM, 114.2 and 118.6 ppm; butatriene, GIAO −0.9 and 85.8 ppm, IGAIM −0.6 and 86.9 ppm.

(9) Wiberg, K. B.; Hammer, J. D.; Zilm, K. W.; Cheeseman, J. R.; Keith, T. A. *J. Phys. Chem.* **1998,** *102A*, 8766.

(10) Bohmann and Farrar (Bohmann, J.; Farrar, T. C. *J. Phys. Chem.* **1996**, *100*, 2646) have analyzed the shielding in acetylenes using a natural bond orbital analysis.

10.1021/jo990423n CCC: $18.00
Published on Web 08/03/1999

Table 2. Calculated and Experimental Shielding, ppm

compound	atom	term	calcd	obsd[a]	compound	atom	term	calcd	obsd[a]
acetylene	C	$\sigma_{xx,yy}$	27	36	pentatetraene	C_2	σ_{xx}	11	
		σ_{zz}	279	276			σ_{yy}	−32	
		σ_{iso}	111	116			σ_{zz}	−5	
allene	CH_2	σ_{xx}	171	163			σ_{iso}	−9	
		σ_{yy}	20	28	pentatetraene	C_3	$\sigma_{xx,yy}$	40	
		σ_{zz}	135	132			σ_{zz}	97	
		σ_{iso}	109	108			σ_{iso}	59	
allene	C	$\sigma_{xx,yy}$	−63	−47	hexapentaene	CH_2	σ_{xx}	169	
		σ_{zz}	3	11			σ_{yy}	10	
		σ_{iso}	−41	−28			σ_{zz}	61	
butatriene	CH_2	σ_{xx}	172				σ_{iso}	80	
		σ_{yy}	15		hexapentaene	C_2	σ_{xx}	19	
		σ_{zz}	64				σ_{yy}	−31	
		σ_{iso}	84				σ_{zz}	−3	
butatriene	C	σ_{xx}	21				σ_{iso}	−5	
		σ_{yy}	−29		hexapentaene	C_3	$\sigma_{xx,yy}$	38	
		σ_{zz}	3				σ_{zz}	17	
		σ_{iso}	−2				σ_{iso}	31	
pentatetraene	CH_2	σ_{xx}	170						
		σ_{yy}	23						
		σ_{zz}	115						
		σ_{iso}	103						

[a] The observed shielding was obtained by subtracting the chemical shift vs TMS (ref 1) from the observed shielding of TMS (186.4 ppm).

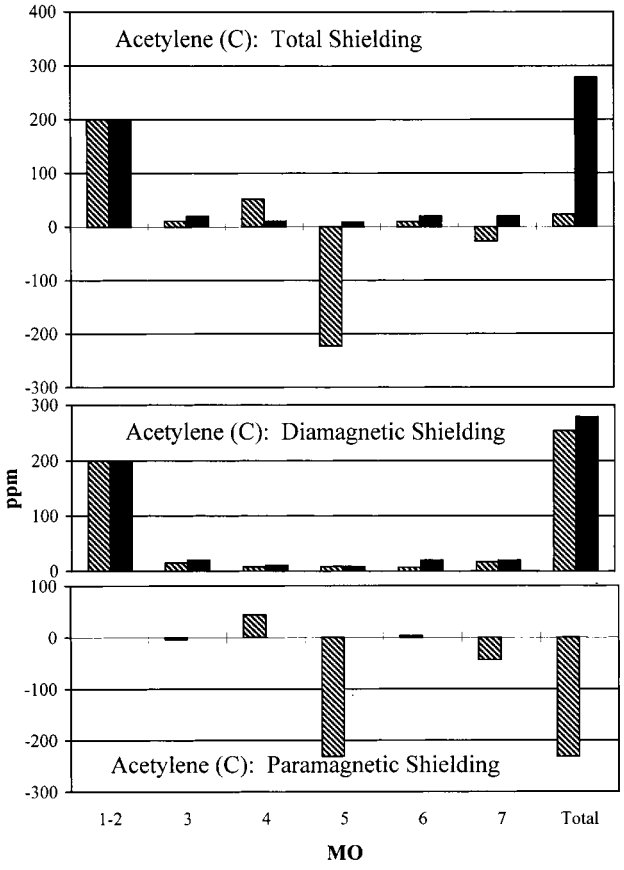

Figure 1. Calculated shielding for acetylene on an MO basis. The hashed bar gives the ⊥ (*x* or *y*) component, and the solid bar gives the || (*z*) component.

The *z*-axis shielding component for the acetylenes arises from the sum of diamagnetic contributions from all of the MOs (Figure 1). As a linear molecule, acetylene has no paramagnetic shielding about the *z* axis.[11] The cylindrical symmetry of the p-π electrons leads to a significant diamagnetic contribution. The *z* axis shift for acetylenes is close to that calculated for C^{4-} and CH_3^-,[12] and represents the maximum diamagnetic shielding at carbon.

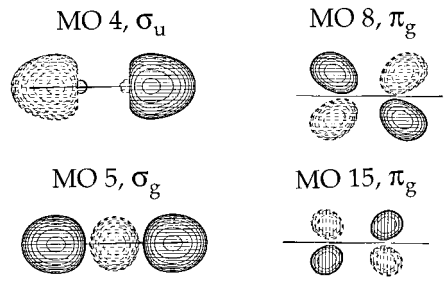

Figure 2. Molecular orbitals of acetylene. MOs 4 and 5 are occupied.

Table 3. Main Contributions to the Paramagnetic Shielding of Acetylene, ppm

occupied MO	atom	virtual MO	σ_{xx}^p
5	C	8	−184
		15	−56

The deshielding (downfield shift) observed about the *x*- and *y*-axes of acetylene results mainly from the σ MO 5 (Figure 2) and its coupling with the π_y* virtual MO 8 (Table 3). In Figure 3 we illustrate how a magnetic field can couple these two MOs to generate paramagnetic shielding. MO 5 consists primarily of two p_z atomic-like orbitals (one centered at each carbon) which overlap to form a bonding σ MO. Quantum mechanically, a magnetic field applied along the *x*-axis (B_x) corresponds to an angular momentum operation about this same axis (L_x). The result of an angular momentum operation on a p orbital is rotation of the orbital 90° about the axis of operation.[13] As shown in Figure 3, when a field is applied

(11) Ramsey, N. F. *Phys. Rev.* **1950**, *78*, 699.

(12) Wiberg, K. B.; Hammer, J. D..; Keith, T. A.; Zilm, K. W *J. Phys. Chem.* **1999**, *103A*, 21.

(13) In general, $L_x(p_y) = p_z$, along with the other five cyclic permutations.

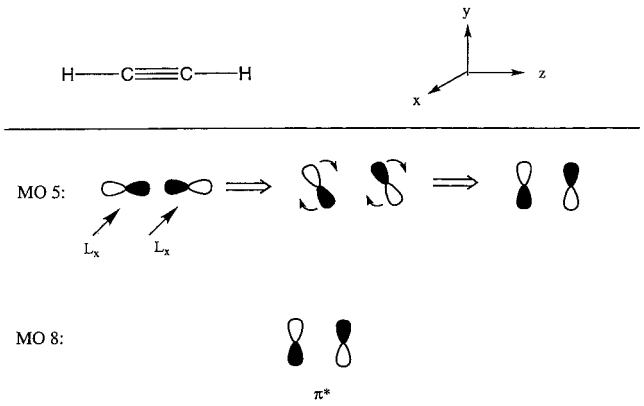

Figure 3. Effect of L_x operating on MO 5 of acetylene.

along *x*, the L_x operator transforms the p_z orbitals of MO 5 into p_y orbitals, resulting in an MO with π_y* symmetry. Because virtual MO 8 has the same symmetry and spatial orientation, it can now couple with MO 5 to contribute paramagnetic shielding. MO 15 is another virtual MO (similar to MO 8 but with additional nodes) which also couples with MO 5, although to a lesser extent.

Although the central carbon in allene and the carbons in the acetylenes make use of the same hybrid orbitals, the shieldings are quite different (Figure 4). The diamagnetic terms for the central allene carbon are similar to those for acetylene, but here, the p-π orbitals lead to large *z*-axis paramagnetic terms. The difference with respect to the acetylenes arises from the fact that although the π orbitals in allene are energetically degenerate, they are not *spatially* degenerate (Figure 5). Thus, whereas it is possible to take linear combinations of the acetylene π orbitals, leading to a cylindrically symmetric electron density distribution, this is not the case with allene.[14] Here, the occupied π orbitals (MOs 10 and 11) couple with virtual MOs 13 and 12, respectively, in the presence of a magnetic field along *z*, leading to a large paramagnetic interaction.

It is also interesting to note that the observed isotropic shift of the central carbon in allene is roughly 140 ppm downfield from that of the terminal carbons. From the plots in Figure 4, one can see that this difference is due in part to the difference in the paramagnetic shielding arising from MO 7. When a field is applied along the *x*-axis, MO 7 gives a paramagnetic shielding of −54 ppm at the CH_2 carbons and −269 ppm at the central carbon. A field applied along the *y*-axis gives −215 ppm at CH_2 and −269 ppm at the central carbon. Another significant difference in shielding between the central and terminal carbons arises from the *z*-axis component from MOs 10 and 11. The paramagnetic contribution from MO 10 along the *z*-axis is −19 at the CH_2 carbon, but −177 ppm for the central carbon. The corresponding contributions from MO 11 are −55 ppm for CH_2 and, again, −177 ppm for the central carbon.[15]

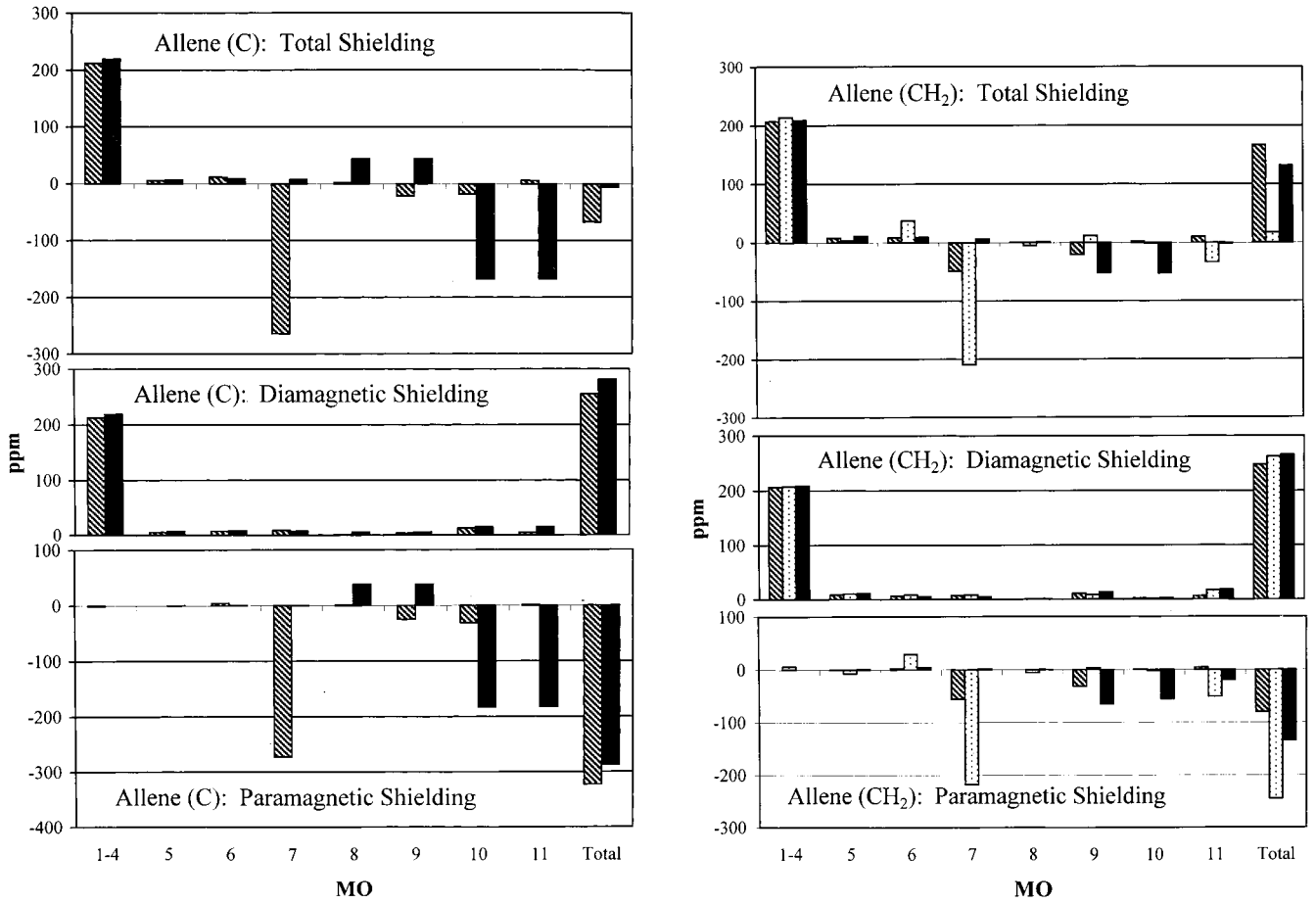

Figure 4. Calculated shielding for allene on an MO basis: (a, left) the central carbon; the hashed bar give the ⊥ (*x* or *y*) component, and the solid bar gives the ∥ (*z*) component; (b, right) the terminal methylene carbon that lies in the *yz* plane; The hashed bar gives the *x* component, the dotted bar gives the *y* component, and the solid bar gives the *z* component.

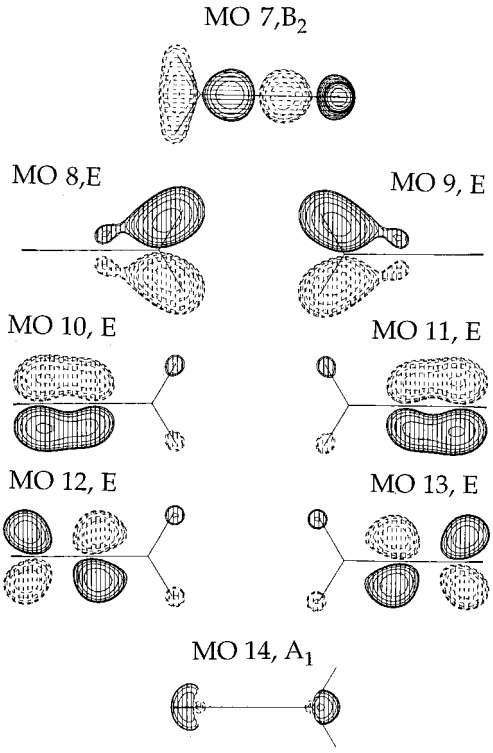

Figure 5. Molecular orbitals of allene. MOs 7−11 are occupied. MOs 7, 9, 11, and 13 lie in the *yz* plane whereas MOs 8, 10, 12, and 14 lie in the *xz* plane.

Table 4. Main Contributions to the Paramagnetic Shielding of Allene, ppm

occupied MO	atom	virtual MO	σ_{xx}^{p}	σ_{yy}^{p}	σ_{zz}^{p}
7	C	12		−242	
		13	−242		
	CH_2	12		−176	
10	C	13			−158

To better understand the origin of these differences, it is important to examine the nature of the occupied and virtual MOs involved in the paramagnetic shielding. Table 4 shows the important occupied-virtual interactions, and Figure 5 shows the key MOs involved in producing paramagnetic shielding for allene. MO 7 is a σ MO composed primarily of p_z atomic-like orbitals centered at each of the three carbons. A field applied along the *x*-axis rotates the p_z orbitals 90° so that they now lie in the *y*-direction:

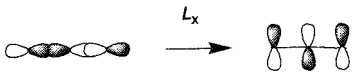

In this orientation the p-orbitals associated with the central and right-hand CH_2 carbons will have significant overlap with virtual MO 13. However, because the p-orbital at the left-hand CH_2 of MO 13 is quite small,[16] its interaction with MO 7 will be minimal. For a field applied along the *y*-axis, the p-orbitals at the central and left-hand CH_2 carbons of MO 12 will have extensive overlap with MO 7, but again, it can be seen that the p-orbitals of the right-hand CH_2 will have little interaction. Thus, the average interaction at a CH_2 carbon will be much less than at the central carbon.

The same rationale can be used to explain the difference in shielding for a field applied along *z*. As described earlier, occupied MOs 10 and 11 couple with virtual MOs 13 and 12, respectively, to generate significant paramagnetic deshielding along *z* at the central carbon. However, MO 10 has a very small p_x orbital coefficient at the right-hand CH_2, and MO 13 has a very small p_y coefficient at the left-hand CH_2. Thus, in the presence of a magnetic field along *z*, the overlap of MO 10 with MO 13 at the CH_2 carbons is small compared with that at the central carbon. The same is true for the MO 11−MO 12 pair. Thus, in allene it appears that the relatively small p-orbital coefficients at the CH_2 carbons in the above orbitals account for much of the difference in shielding between the central and the CH_2 carbons.

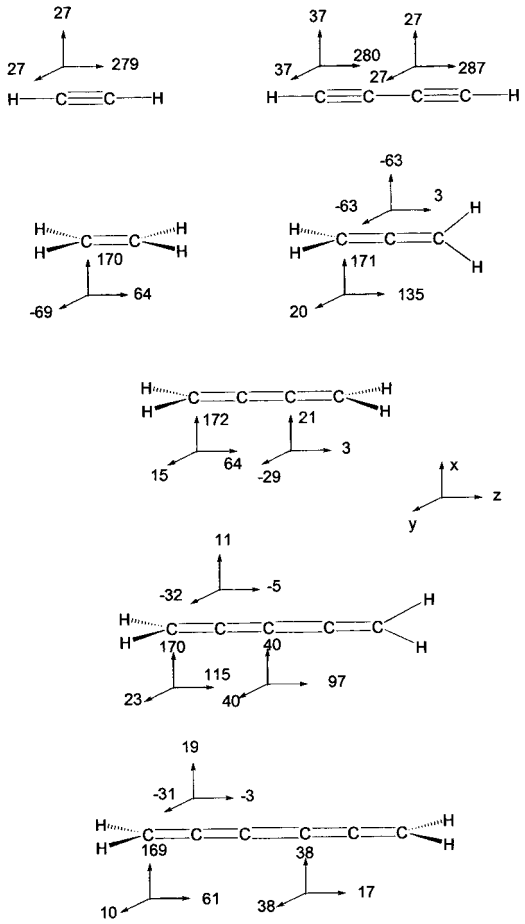

Figure 6. Calculated tensor components of the shielding at carbon.

Higher Cumulenes

Are the shifts for allene characteristic of the higher cumulenes such as butatriene (**3**), pentatetraene (**4**), and hexapentaene (**5**)? The NMR spectra of these compounds have not been reported, but they may be calculated (Table 2, Figure 6). The *z*-axis components for all of the carbons are shifted downfield. On the other hand, the higher

(14) A similar description has been given by J. Grutzner (*Recent Advances in Organic NMR Spectroscopy*; Lambert, J. B., Rittner, R., Eds.; UNICAMP: Campinas, Brazil, 1987.

(15) Because of the local cylindrical symmetry at the central allenic carbon, the same shielding will be derived from a field along any direction perpendicular to the *z*-axis.

(16) Although there is a small p_y orbital coefficient at this carbon, it is not visible in Figure 5 at the contour level at which these plots were generated.

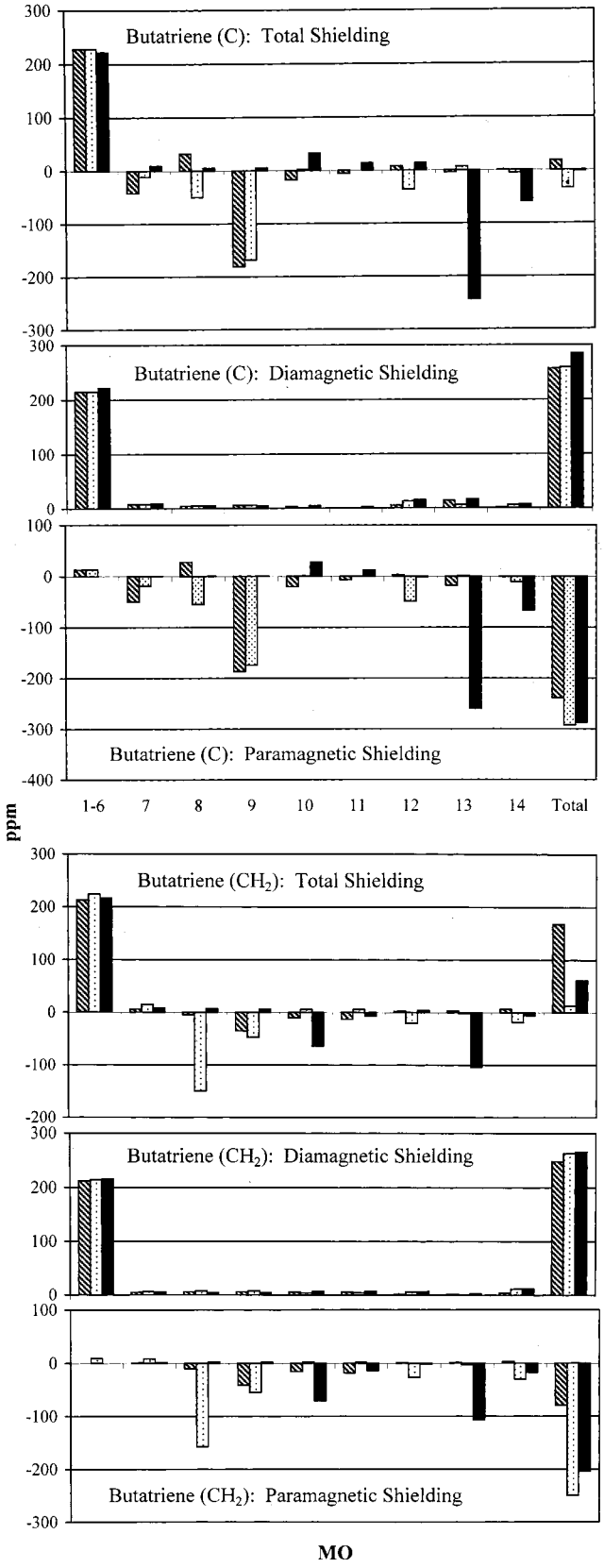

Figure 7. Calculated shielding for butatriene on an MO basis. The molecule lies in the *yz* plane, and *x* is out-of-plane.

acetylenes, such as diacetylene,[17] maintain their upfield shift about the *z*-axis.

It can be seen that there are differences in the *z*-axis shielding components for the cumulenes. Here it may be noted that there are two groups of cumulenes. The CH_2 groups of odd-membered cumulenes lie in planes that are perpendicular to each other to give overall D_{2d} symmetry, and have sets of energetically degenerate π MOs. The CH_2 groups of the even-membered cumulenes are coplanar, and they belong to the D_{2h} point group. Here, there are two sets of nondegenerate π MOs having different numbers of p-orbitals. One might then think that the cumulenes belonging to one group would show a different pattern of shielding from that of the cumulenes in the other group. For example, the CH_2 shielding tensors in allene and pentatetraene are quite similar (Table 2).

However, the central carbon (C_3) of pentatetraene is unlike the central carbon of allene, and although one might expect the C_2 carbons of butatriene and pentatetraene to be different, they are actually quite similar. So there does not appear to be any clear pattern of shielding within these two groups of cumulenes. There is, however, at least one general shielding trend among the first four cumulenes: The internal carbons are always less shielded

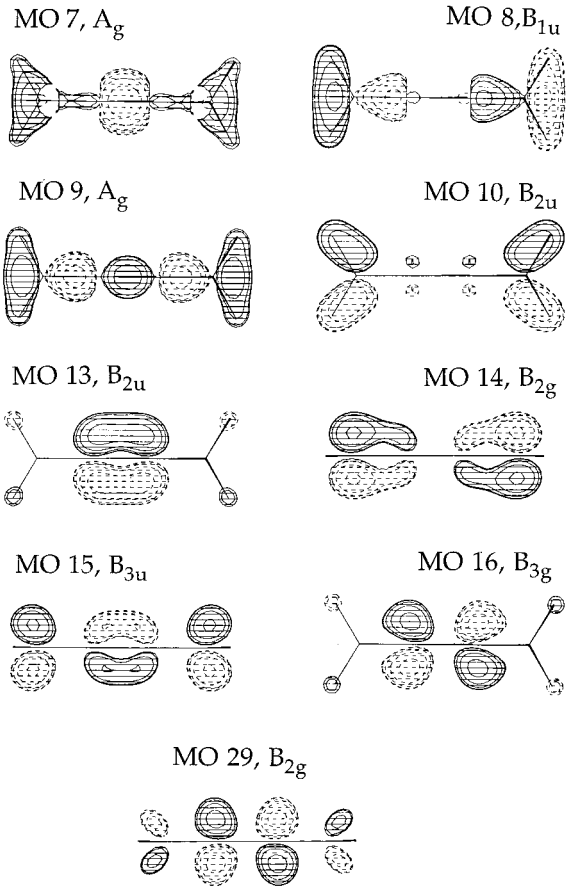

Figure 8. Molecular orbitals of butatriene. MOs 7−14 are occupied. MOs 7−10, 13, and 16 lie in the *yz* plane, and MOs 14, 15, and 29 lie in the *xz* plane.

Table 5. Main Contributions to the Paramagnetic Shielding of Butatriene, ppm

occupied MO	atom	virtual MO	σ_{xx}^{p}	σ_{yy}^{p}	σ_{zz}^{p}
9	C	16	−168		
		29		−140	
	CH_2	29		−108	
13	C	15			−251
	CH_2	15			−106
14	C	16			−55

(17) Cf. ref 1 for a comparison of acetylene and diacetylene.

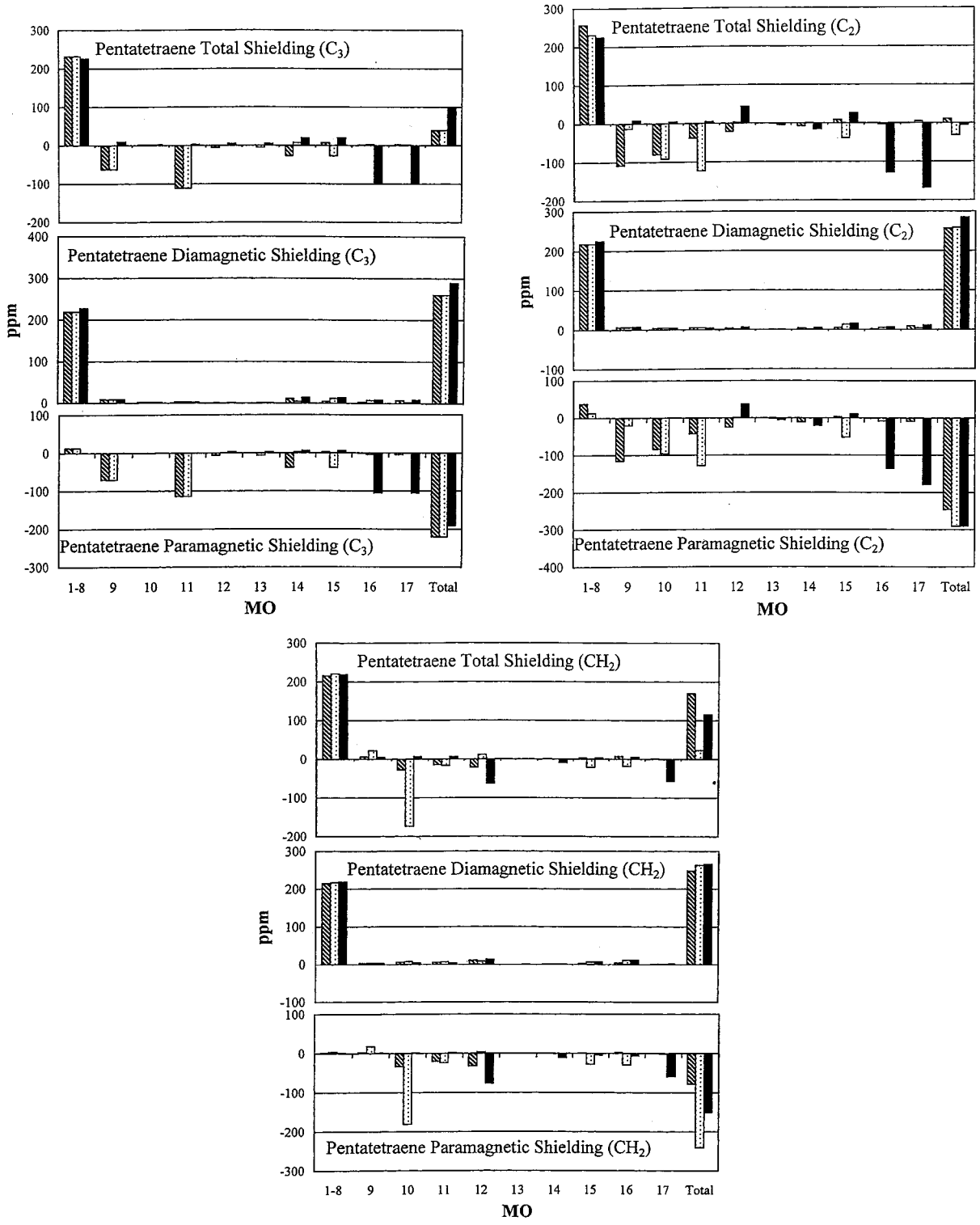

Figure 9. Calculated shielding of pentatetraene on an MO basis: (a, top left) the central carbon; (b, top right) C_2; (c, bottom) the terminal methylene carbon that lies in the *yz* plane.

than the terminal CH_2 carbons. In butatriene, the isotropic shielding of the internal carbons is smaller by ~85 ppm than that of the terminal carbons. Similarly, the isotropic shieldings of C_2 and C_3 in pentatetraene are ~110 and ~45 ppm smaller, respectively, than that for the CH_2 carbon.

The explanation for this pattern is quite similar to that described for allene. Figure 7 shows the shielding for butatriene on an MO basis, and Figure 8 shows the relevant MOs. A comparison of the paramagnetic shielding contributions for the two different carbons shows that, for a magnetic field along *x* and *y*, MO 9 gives over 100 ppm greater paramagnetic deshielding to the internal carbons than the CH_2 carbons. Table 5 shows the major occupied-virtual MO interactions which lead to the paramagnetic terms, and it can be seen that, for a field applied along *y*, occupied MO 9 mixes with virtual MO 29 to give large paramagnetic deshielding contributions at both the internal and CH_2 carbons. However, while a field applied along *x* couples MO 9 with MO 16 to give

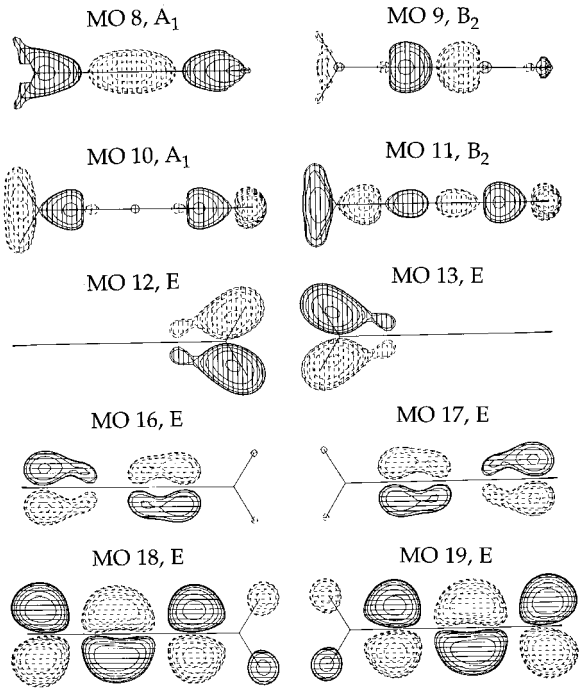

Figure 10. Molecular orbitals of pentatetraene. MOs 8−17 are occupied. MOs 8−11, 13, 17, and 18 lie in the *yz* plane, and MOs 12, 16, and 19 lie in the *xz* plane.

substantial deshielding at the internal carbons, no paramagnetic deshielding is generated at the CH_2 carbons. As with allene, the p-orbitals associated with the CH_2 carbons in MO 16 are quite small in comparison with those centered at the internal carbons. Thus, the magnitude of the coupling involving the CH_2 p-orbitals will be correspondingly small. From an inspection of the MO plots in Figure 10, it is apparent that this description also applies to pentatetraene.

One may ask why the shielding tensors at C_2 and C_3 of pentatetraene are so different. In particular, the *z*-axis tensor component at C_2 is calculated to be over 100 ppm less shielded than the *z*-component at C_3. The primary source of the difference in the shielding along *z* is occupied MOs 16 and 17 (Figure 9). Table 6 shows that MO 16 couples with MO 18 to give ∼30 ppm more paramagnetic deshielding at C_2 than at C_3, and MO 17 couples with MO 19 to give ∼70 ppm more paramagnetic deshielding at C_2 relative to C_3. In MO 17, the p-orbital coefficient at C_2 is greater than that at C_3 whereas in MO 19 the two p_y coefficients are similar (Figure 10). This leads to significantly greater paramagnetic deshielding at C_2 than at C_3. In MO 16 the p_x coefficient is slightly smaller at C_2 than at C3, but in MO 18 the p_y coefficient is significantly larger at C_2 than at C_3. Therefore, the paramagnetic interaction resulting from these MOs will give the larger deshielding effect at C_2.

Table 6. Main Contributions to the Paramagnetic Shielding of Pentatetraene, ppm

occupied MO	atom	virtual MO	σ_{xx}^p	σ_{yy}^p	σ_{zz}^p
10	C_1	19		−232	
	C_2	18	−136		
	C_2	19		−121	
16	C_2	18			−136
	C_3	18			−107
17	C_1	19			−58
	C_2	19			−172
	C_3	19			−107

In the *x*- and *y*-directions, MO 10 contributes −84 and −96 ppm, respectively, to the shielding at C_2. However, MO 10 does not give a paramagnetic contribution to C_3. Here, the MO plots are unambiguous. MO 10 is composed of p_z orbitals that are centered primarily at C_1 and C_2. A field applied along *y*, for example, rotates the p_z orbital centered at C_2 into a p_x orbital which can now mix with the corresponding p_x orbital in virtual MO 19. Since MO 10 has almost no orbital amplitude at C_3, its interaction with MO 19 is negligible at this carbon.

Conclusions

The strong *z*-axis shielding of acetylene arises from its lack of paramagnetic shielding, and from the extra diamagnetic shielding that arises from its energetically and spatially degenerate π orbitals. Allene also has energetically degenerate π orbitals, but since they are not spatially degenerate, they do not give diamagnetic shielding, but rather they couple with virtual orbitals to give paramagnetic deshielding.

The large difference in isotropic shielding between the methylene carbons and the central carbon of allene is a result of the differences in p-orbital coefficients among the occupied orbitals and the virtual orbitals with which they couple in the presence of a magnetic field. The differences among the cumulenes may also be directly attributed to the nature of the MOs.

Calculations

The shielding calculations were carried out using Gaussian-95.[18] The MO analysis was carried out using a modified version of Gaussina-95.

Acknowledgment is made to the donors of the Petroleum Research Fund, administered by the ACS, for support of this work.

JO990423N

(18) Frisch, M. J.; Trucks; G. W.; Schlegel, H. B.; Gill, P. M. W.; Johnson, B. G.; Robb; M. A.; Cheeseman, J. R.; Keith, T.; Petersson, G. A.; Montgomery, J. A.; Raghavachari, K.; Al-Laham, M. A.; Zakrzewski, V. G.; Ortis, J. V.; Foresman, J. B.; Cioslowski, J.; Sefanov, B. B.; Nanayakkara, A.; Challacombe, M.; Peng, C. Y.; Ayala, P. Y.; Chen, W.; Wong, M. W.; Andres, J. L.; Replogle, E. S.; Gomperts, R.; Martin, R. L.; Fox, D. J.; Binkley, J. S.; Defrees, D. J.; Baker, J.; Stewart, J. P.; Head-Gordon, M.; Gonzalez, C.; Pople, J. A. *Gaussian 95*, Development Version (Rev. D); Gaussian, Inc.: Pittsburgh, PA, 1995.